

Spherical harmonic analysis and synthesis using FFT: Application to temporal gravity variation[☆]

Cheinway Hwang*, Yu-Chi Kao

Department of Civil Engineering, National Chiao Tung University, 1001 Ta Hsueh Road, Hsinchu 300, Taiwan

Received 2 February 2005; received in revised form 2 July 2005; accepted 14 July 2005

Abstract

FFT and complex algebra-based methods of spherical harmonic analysis and synthesis are presented. Two computer programs in FORTRAN are developed based on the methods. Both general and special cases are discussed. Special cases involve the analyses of gravity changes of the hydrological origin and the atmospheric origin. Functionals of the Earth's gravity field such as gravity anomaly and geoidal height can also be computed via synthesis. Thermal-corrected sea level anomaly from TOPEX/Poseidon and atmospheric pressure from ECMWF are used to compute changes of geopotential coefficients due to oceanic and atmospheric mass redistributions. Interesting phenomena in the changes of geopotential coefficients have been identified. The two computer programs can facilitate analyses and syntheses of gravity products from satellite missions such as GRACE.

© 2005 Elsevier Ltd. All rights reserved.

Keywords: FFT; Geoid; J_2 ; Spherical harmonics; Temporal gravity

1. Introduction

Spherical harmonic analysis is a process of decomposing a function on a sphere into components of various wavelengths using surface spherical harmonics as base functions. Spherical synthesis combines components of various wavelengths to generate function values on a sphere and is the reverse process of harmonic analysis. Spherical harmonic analysis and synthesis have been used in many occasions, e.g., ocean dynamic topography (Engelis, 1985) and the Earth's static gravity field (Lemoine et al., 1998) and temporal gravity fields

(Wahr et al., 1998). In particular, the temporal variation of the Earth's gravity field is closely related to global climate change. Satellite missions such as GRACE (Tapley et al., 2004) have now routinely delivered products that can be used to derive gravity variations. Spherical harmonic analysis and synthesis are important tools for investigating these gravity variations.

Existing works on spherical harmonic analysis and synthesis can be found in, e.g., Colombo (1981), Dilts (1985), Potts et al. (1998), Mohlenkamp (1999), Kostelec et al. (2000), Suda and Takami (2002) and Healy et al. (2003). There are two procedures in doing spherical harmonic analysis and synthesis. One procedure is based on numerical integration and the other based on least-squares (e.g., Colombo, 1981). Both spherical harmonic analysis (using numerical integration) and synthesis can take advantage of fast Fourier transform (FFT). For example, Colombo (1981) and Dilts (1985) have developed algorithms for spherical harmonic analysis using

[☆]Code on server at <http://www.iamg.org/CGEditor/index.htm>

*Corresponding author. Tel.: +88 63 5724739;
fax: +88 63 5716257

E-mail address: hwang@geodesy.cv.nctu.edu.tw
(C. Hwang).

FFT. In this paper, we will present two efficient, FFT-based computer programs for spherical harmonic analysis and synthesis. Our methods will still employ FFT but we will use different algorithms and the complex algebra. We will emphasize special cases involving the temporal variation of the Earth’s gravity field. Sea level data and atmospheric data will be used to compute gravity variations and to demonstrate the usages of the computer programs.

2. Spherical harmonic analysis

2.1. General case

Any spherical function, $f(\phi, \lambda)$, can be expanded into series of surface spherical harmonics (Heiskanen and Moritz, 1985) as

$$f(\theta, \lambda) = \sum_{n=0}^{\infty} \sum_{m=0}^n [\bar{a}_{nm} \bar{R}_{nm}(\theta, \lambda) + \bar{b}_{nm} \bar{S}_{nm}(\theta, \lambda)], \quad (1)$$

where \bar{a}_{nm} and \bar{b}_{nm} are harmonic coefficients, θ and λ are co-latitude (polar distance angle from the north pole) and geocentric longitude, respectively, $\bar{R}_{nm} = \bar{P}_{nm}(\cos \theta) \cos m \lambda$ and $\bar{S}_{nm} = \bar{P}_{nm}(\cos \theta) \sin m \lambda$ are fully normalized spherical harmonics, $\bar{P}_{nm}(\cos \theta)$ is the fully normalized associated Legendre function, and n and m are degree and order, respectively. In a continuous case, \bar{a}_{nm} and \bar{b}_{nm} can be obtained using the orthogonal relationship of spherical harmonics as (Heiskanen and Moritz, 1985, p. 29)

$$\begin{Bmatrix} \bar{a}_{nm} \\ \bar{b}_{nm} \end{Bmatrix} = \frac{1}{4\pi} \int_{\lambda=0}^{2\pi} \int_{\theta=0}^{\pi} f(\theta, \lambda) \begin{Bmatrix} \bar{R}_{nm} \\ \bar{S}_{nm} \end{Bmatrix} \sin \theta \, d\theta \, d\lambda. \quad (2)$$

In practice, function values of f are always given at discrete points, so (2) can only be implemented numerically and approximately. Let $t = \cos \theta$ and $C_{nm} = (\bar{a}_{nm} + i\bar{b}_{nm})$, where $i = \sqrt{-1}$. Given f on a global, regular $\Delta\theta \times \Delta\lambda$ grid ($\Delta\theta$ is the sampling interval in latitude and $\Delta\lambda$ is the sampling interval in longitude), (2) can be approximated as (Hwang, 2001)

$$\begin{aligned} C_{nm} &= \frac{1}{4\pi q_n} \sum_{k=1}^{M-1} \sum_{l=1}^{N-1} \bar{f}(\theta_k, \lambda_l) \\ &\quad \times \left[\int_{t_k}^{t_{k+1}} \bar{P}_{nm}(t) \, dt \right] \left[\int_{\lambda_l}^{\lambda_{l+1}} e^{im\lambda} \, d\lambda \right] \\ &= \frac{g_m}{4\pi q_n} \sum_{k=1}^{M-1} I \bar{P}_{nm}^k \sum_{l=1}^{N-1} \bar{f}(\theta_k, \lambda_l) e^{i2\pi m(l-1)/(N-1)} \\ &= \frac{g_m}{4\pi q_n} \sum_{k=1}^{(M-1)/2} I \bar{P}_{nm}^k [\bar{f}_k(m) + (-1)^{n-m} \bar{f}_{M-k}(m)], \quad (3) \end{aligned}$$

$$g_m = \begin{cases} \Delta\lambda, & \text{if } m = 0, \\ [\sin(m\Delta\lambda) + i(1 - \cos(m\Delta\lambda))]/m & \text{if } m \neq 0, \end{cases} \quad (4)$$

where $M = (\pi/\Delta\theta + 1)$ is the number of grids in latitude and $N = (2\pi/\Delta\lambda + 1)$ is the number of grids in longitude, $t_k = \cos((k-1)\Delta\theta)$, $\lambda_l = (l-1)\Delta\lambda$, $I \bar{P}_{nm}^k$ is the integration of associated Legendre function (Paul, 1978), q_n is a quantity dependent on n and the block size $\bar{f}(\theta_k, \lambda_k)$ (Rapp, 1989, p. 266) and is to make the approximation in (3) to (2) as realistic as possible. Colombo (1981, p. 76) suggested that q_n be set to:

$$\begin{aligned} q_n &= \beta_n^2, & 0 \leq n \leq L/3, \\ q_n &= \beta_n, & N/3 < n < L, \\ q_n &= 1, & n > L, \end{aligned} \quad (5)$$

where β_n is the Pellinen smoothing factor given by

$$\beta_n = \frac{1}{1 - \cos \psi_0} \frac{1}{\sqrt{2n+1}} [P_{n-1}(\cos \psi_0) - P_{n+1}(\cos \psi_0)] \quad (6)$$

with L being the maximum degree of expansion and ψ_0 being the radius of a spherical cap whose area is the same as the block size of $\bar{f}(\theta_k, \lambda_k)$. The last equation in (3) is due to the fact that $I \bar{P}_{nm}^{M-k} = (-1)^{n-m} I \bar{P}_{nm}^k$. As such, the integration of associated Legendre functions needs to be done only for the northern hemisphere. In (3), \bar{f} is the mean value in a block (or cell) and is computed by the four-point average as

$$\begin{aligned} \bar{f}(\phi_k, \lambda_l) &= \frac{1}{4} [f(k\Delta\theta, l\Delta\lambda) + f((k+1)\Delta\theta, l\Delta\lambda) \\ &\quad + f((k+1)\Delta\theta, (l+1)\Delta\lambda) \\ &\quad + f(k\Delta\theta, (l+1)\Delta\lambda)]. \quad (7) \end{aligned}$$

In (3), let $K = N - 1 =$ number of blocks in longitude, $p = l - 1$. Then we have

$$\bar{f}_k(m) = \sum_{p=0}^{K-1} \bar{f}(\phi_k, \lambda_l) e^{i2\pi mp/K}, \quad m = 0, \dots, K-1, \quad (8)$$

which can be computed efficiently by FFT for all m . The maximum degree of expansion L follows the rule that $L = \pi/\Delta\theta$ (Rapp, 1989). Since $L < K - 1$, for each fixed k we will need the $\bar{f}_k(m)$ values in (8) only up to $m = L$. In our programming, the computations start from the northernmost and southernmost latitude belts simultaneously and converge to the equator. The mean block values (see (7)) from the northern and southern hemisphere are stored in a complex array (one in the real part and the other in the imaginary part), which is then Fourier transformed to form the two needed Fourier arrays. This process of simultaneously Fourier transforming two real-valued arrays significantly reduces the computing time as compared to the process of transforming real-valued array one by one.

2.2. Case for variation of Earth’s gravity field

Mass variation within the Earth system may be induced by changes in ocean, atmosphere, precipitation (snow and rainfall), water table, glacier, ice sheet, etc. The origins of mass changes (Δm) may be classified into two categories. One is of the hydrological origin and in this case mass variation is related to the density of the underlying quantity and the change of height (or thickness). The other is of the pressure origin and in this case mass variation is related to the change of pressure. At any point (r, θ, λ) (r : geocentric distance) exterior to the Earth, the perturbing potential relative to a static Earth caused by surface mass variations on a sphere of radius R can be expressed as

$$\begin{Bmatrix} \Delta V^h(r, \theta, \lambda) \\ \Delta V^p(r, \theta, \lambda) \end{Bmatrix} = G \iint_{\sigma} \frac{1}{s} \begin{Bmatrix} \rho \Delta h \\ \Delta p/g \end{Bmatrix} d\sigma, \quad (9)$$

where $d\sigma = R^2 \sin \theta d\theta d\lambda$, s is the distance from a surface area element to point (r, θ, λ) , ΔV^h is the perturbing potential due to Δh (hydrological origin), and ΔV^p is the perturbing potential due to Δp (pressure origin). The perturbing potential can be used to derive variations in gravity, geoid, deflection of the vertical and other functionals of the Earth’s gravity field. It turns out that conversion between surface mass variations and perturbing potentials in the spherical harmonic domain is much easier than conversion in the space domain as expressed in (9). First, a perturbing potential in (9) can be represented by a series of spherical harmonics as

$$\Delta V^i(r, \theta, \lambda) = \frac{GM}{r} \sum_{n=0}^{\infty} \left(\frac{a}{r}\right)^n \sum_{m=0}^n \times \left[\Delta \bar{J}_{nm}^i \bar{R}_{nm}(\theta, \lambda) + \Delta \bar{K}_{nm}^i \bar{S}_{nm}(\theta, \lambda) \right], \quad (10)$$

where $\Delta \bar{J}_{nm}^i$ and $\Delta \bar{K}_{nm}^i$ are changes of geopotential coefficients, $i = \Delta h$ or Δp , and a is a constant that is roughly equal to the semi-major axis of the Earth’s reference ellipsoid. The inverse of distance s can also be expanded into a series of spherical harmonics as

$$\frac{1}{s} = \frac{1}{r} \sum_{n=0}^{\infty} \frac{1}{2n+1} \left(\frac{a}{r}\right)^n \sum_{m=0}^n \times \left[\bar{R}_{nm}(\theta', \lambda') \bar{R}_{nm}(\theta, \lambda) + \bar{S}_{nm}(\theta', \lambda') \bar{S}_{nm}(\theta, \lambda) \right], \quad (11)$$

where (θ', λ') are the spherical coordinates of a surface area element. Since Δh and Δp are functions on a sphere, they can also be expanded into series of spherical harmonics (Section 2.1):

$$\Delta h(\theta, \lambda) = \sum_{n=0}^{\infty} \sum_{m=0}^n \left[\bar{a}_{nm}^h \bar{R}_{nm}(\theta, \lambda) + \bar{b}_{nm}^h \bar{S}_{nm}(\theta, \lambda) \right], \quad (12)$$

$$\Delta p(\theta, \lambda) = \sum_{n=0}^{\infty} \sum_{m=0}^n \left[\bar{a}_{nm}^p \bar{R}_{nm}(\theta, \lambda) + \bar{b}_{nm}^p \bar{S}_{nm}(\theta, \lambda) \right], \quad (13)$$

Substituting (11), (12) and (13) into (9) and considering surface loading effects leads to

$$\begin{Bmatrix} \Delta \bar{J}_{nm}^h \\ \Delta \bar{K}_{nm}^h \end{Bmatrix} = \frac{4\pi \rho a^2 (1 + k_n)}{M(2n + 1)} \begin{Bmatrix} \bar{a}_{nm}^h \\ \bar{b}_{nm}^h \end{Bmatrix}, \quad (14)$$

$$\begin{Bmatrix} \Delta \bar{J}_{nm}^p \\ \Delta \bar{K}_{nm}^p \end{Bmatrix} = \frac{4\pi a^2 (1 + k_n)}{gM(2n + 1)} \begin{Bmatrix} \bar{a}_{nm}^p \\ \bar{b}_{nm}^p \end{Bmatrix}, \quad (15)$$

where $(\Delta \bar{J}_{nm}^h, \Delta \bar{K}_{nm}^h)$ are changes of geopotential coefficients derived from Δh , $(\Delta \bar{J}_{nm}^p, \Delta \bar{K}_{nm}^p)$ are coefficients from Δp , k_n is the loading Love number of degree n (see, e.g., Han and Wahr, 1995), and M is the mass of the Earth ($\approx 5.973 \times 10^{24}$ kg). In deriving (14) and (15) the orthogonal relationships of spherical harmonics are used. Eqs. (14) and (15) express the relationships between mass variations and perturbing potentials in the spherical harmonic domain. In (14) and (15), the coefficients $\bar{a}_{nm}^h, \bar{b}_{nm}^h, \bar{a}_{nm}^p,$ and \bar{b}_{nm}^p are derived from global gridded data on a sphere with a radius of a . Note that the geopotential coefficients are unitless and hence care must be exercised in using the units for pressure and height change. Specifically, if $g, M, a,$ and ρ are in SI units, Δh should be in meter and Δp should be in hpa (i.e., $\text{kg m}^{-1} \text{s}^{-2}$).

3. Spherical harmonic synthesis

3.1. General case

Given spherical harmonic coefficients, harmonic synthesis is to generate function values on a global $\Delta\theta \times \Delta\lambda$ grid as (see (1))

$$f(k\Delta\theta, l\Delta\lambda) = \sum_{n=0}^L \sum_{m=0}^n \times \left[\bar{a}_{nm} \bar{R}_{nm}(k\Delta\theta, l\Delta\lambda) + \bar{b}_{nm} \bar{S}_{nm}(k\Delta\theta, l\Delta\lambda) \right], \quad k = 0, \dots, M, l = 0, \dots, N - 1. \quad (16)$$

It is clear that $f(k\Delta\theta, N\Delta\lambda) = f(k\Delta\theta, 0)$, i.e., the values at longitude = 360° and 0° are identical. To facilitate the application of FFT, (16) is re-written as

$$f(k\Delta\theta, l\Delta\lambda) = \sum_0^L \left\{ \left[\sum_{n=m}^L \bar{P}_{nm}(k\Delta\theta) \bar{a}_{nm} \right] \cos(ml\Delta\lambda) + \left[\sum_{n=m}^L \bar{P}_{nm}(k\Delta\theta) \bar{b}_{nm} \right] \sin(ml\Delta\lambda) \right\} = \sum_0^L (C_m \cos(ml\Delta\lambda) + S_m \sin(ml\Delta\lambda)) \quad k = 0, \dots, M, l = 0, \dots, N - 1. \quad (17)$$

Note $S_0 = 0$. In (15), let $C_m = S_m = 0$ for $m = L + 1, \dots, N - 1$, and

$$B_m = \frac{C_m - iS_m}{2}. \tag{18}$$

Then

$$\begin{aligned} f(k\Delta\theta, l\Delta\lambda) &= 2 \operatorname{Re} \left(\sum_{m=0}^{N-1} B_m e^{i2\pi mlk/N} \right) \\ &= 2 \operatorname{Re}(P), l = 0, \dots, N - 1, \end{aligned} \tag{19}$$

where Re stands for the real part of a complex number. In (19), the sum P can be evaluated for all gridded values along the same parallel (co-latitude = $k\Delta\theta$) by FFT. Because the associated Legendre function satisfies

$$\bar{P}_{nm}(-t) = (-1)^{n-m} \bar{P}_{nm}(t), \tag{20}$$

$\Delta\theta$ should be so chosen that 90° is an integer multiplier of $\Delta\theta$. In this case, the associated Legendre functions need to be computed only for the northern hemisphere, and they can be used for the southern hemisphere with only a selected change of sign based on the rule in (20); see also Colombo (1981).

3.2. Case for functional of the Earth's gravity field

Given a set of geopotential coefficients, we can compute any functional of the gravity field. For example, geoidal height (or variation of geoidal height) can be expanded into a series of spherical harmonics as

$$\begin{aligned} \zeta(R, \theta, \lambda) &= \frac{GM}{R\gamma} \sum_{n=2}^{\infty} \left(\frac{a}{R}\right)^n \sum_{m=0}^n \\ &\quad \times [\bar{J}_{nm} \bar{R}_{nm}(\theta, \lambda) + \bar{K}_{nm} \bar{S}_{nm}(\theta, \lambda)] \\ &= \sum_{m=0}^L \left\{ \left[\sum_{n=m}^L \frac{GM}{R\gamma} \left(\frac{a}{R}\right)^n \bar{P}_{nm}(\theta) \bar{J}_{nm} \right] \cos(m\lambda) \right. \\ &\quad \left. + \left[\sum_{n=m}^L \frac{GM}{R\gamma} \left(\frac{a}{R}\right)^n \bar{P}_{nm}(\theta) \bar{K}_{nm} \right] \sin(m\lambda) \right\} \\ &= \sum_{m=0}^L (C_m^\zeta \cos(m\lambda) + S_m^\zeta \sin(m\lambda)), \end{aligned} \tag{21}$$

where ζ is the geoidal height and R is the radius of the sphere where the expansion is made. Likewise, gravity anomaly (or variation of gravity anomaly) can be expanded into a series of spherical harmonics as

$$\Delta g(R, \theta, \lambda) = \frac{GM}{R^2} \sum_{n=2}^{\infty} (n-1) \left(\frac{a}{R}\right)^n \sum_{m=0}^n$$

$$\begin{aligned} &\times [\bar{J}_{nm} \bar{R}_{nm}(\theta, \lambda) + \bar{K}_{nm} \bar{S}_{nm}(\theta, \lambda)] \\ &= \sum_{m=0}^L \left\{ \left[\sum_{n=m}^L \frac{GM}{R^2} (n-1) \left(\frac{a}{R}\right)^n \bar{P}_{nm}(\theta) \bar{J}_{nm} \right] \cos(m\lambda) \right. \\ &\quad \left. + \left[\sum_{n=m}^L \frac{GM}{R^2} (n-1) \left(\frac{a}{R}\right)^n \bar{P}_{nm}(\theta) \bar{J}_{nm} \right] \sin(m\lambda) \right\} \\ &= \sum_{m=0}^L (C_m^g \cos(m\lambda) + S_m^g \sin(m\lambda)). \end{aligned} \tag{22}$$

One can see in (21) and (22) that, by properly scaling the geopotential coefficients, the algorithm of harmonic synthesis presented in Section 3.1 can be used for syntheses of gravity functionals. Also, the values of functionals are not limited to the surface of the Earth; rather they can be extended to an arbitrary height defined by R . The definitions of geopotential coefficients in (21) and (22) must be clarified here. If the coefficients of gravity variation (see (14) and (15)) are given, then one can use (21) and (22) directly to compute variations of geoidal height and gravity anomaly. If the full geopotential coefficients are given, one must first subtract geopotential coefficients of a reference ellipsoid (see, e.g., Torge, 1989) from the full coefficients, the differences of coefficients are then used in (21) and (22).

If the rates of geopotential coefficients are available, the rates of geoidal height and gravity anomaly can be computed as

$$\begin{aligned} \dot{\zeta}(R, \theta, \lambda) &= \frac{GM}{R\gamma} \sum_{n=2}^{\infty} \left(\frac{a}{R}\right)^n \sum_{m=0}^n \\ &\quad \times [\dot{\bar{J}}_{nm} \bar{R}_{nm}(\theta, \lambda) + \dot{\bar{K}}_{nm} \bar{S}_{nm}(\theta, \lambda)], \end{aligned} \tag{23}$$

$$\begin{aligned} \Delta \dot{g}(R, \theta, \lambda) &= \frac{GM}{R^2} \sum_{n=2}^{\infty} (n-1) \left(\frac{a}{R}\right)^n \sum_{m=0}^n \\ &\quad \times [\dot{\bar{J}}_{nm} \bar{R}_{nm}(\theta, \lambda) + \dot{\bar{K}}_{nm} \bar{S}_{nm}(\theta, \lambda)], \end{aligned} \tag{24}$$

where $\dot{\bar{J}}_{nm}$ and $\dot{\bar{K}}_{nm}$ are the rates of geopotential coefficients. Again, in order to use FFT for an efficient computation, the expressions in (23) and (24) can be changed to forms similar to those in (21) and (22).

4. Computer programs

Two computer programs, coded in FORTRAN90, were developed for spherical harmonic analysis and synthesis in various cases. Program sha is for analysis and syn is for synthesis. Program sha accepts three types of global grid: height anomaly, pressure anomaly, and arbitrary surface function. Program syn reads fully normalized harmonic coefficients to generate a global grid. The format of a global grid is called grd3. A program, z2grd3, is developed to convert a netcdf grid of GMT (Wessel and Smith, 1995) to a grd3 grid. The

computed harmonic coefficients can be either in the fully normalized form or the non-normalized form. The default loading Love numbers are from Han and Wahr (1995) and the maximum available degree is 696. Users can supply their own Love numbers to program sha. Appendix A shows the usages of sha and syn. Appendix B and C show sample batch jobs of analysis and synthesis.

5. Case studies

5.1. Altimeter and atmosphere data

Here we present two case studies using satellite altimeter and atmospheric data. The altimeter data are from the TOPEX/Poseidon (T/P) mission and the data are supplied by AVISO (1996). T/P altimeter data contain sea level anomalies (SLAs) at a 10-day interval and cover a period from January 1993 to October 2001 (from T/P cycle 10 to cycle 344). The thermal-induced sea level change, called steric height, represents the volume change of the oceans and does not introduce mass variation. Therefore, we subtracted the steric heights from SLAs to create corrected sea level anomalies (CSLAs), which reflect oceanic mass change. The steric heights were supplied by Jianli Chen (2003, private communication) at a 10-day interval and cover the same time span as T/Ps; see also Chen et al. (2004) for the modeling of the steric heights. For each T/P cycle, we created a global $1^\circ \times 1^\circ$ grid from the along-track CSLAs. SLAs beyond $\pm 66^\circ$ latitude were padded

with zeroes. The interpolation of SLAs onto a global grid is done by “surface” of GMT. GMTs module `grd2xyz` and program `z2grd3` developed in this paper were used to convert the netcdf grid to `grd3` suitable for use in sha. In order to reduce data noises, monthly SLAs were created and were used in this paper. As an example, Fig. 1 shows CSLAs in December 1997. As seen in Fig. 1, during the 1997–1998 El Niño the oceanic mass increased in the equatorial, eastern Pacific Ocean and decreased in the western Pacific Ocean. The maximum changes of sea level in these two areas reach 40 cm. Large changes of ocean mass also occurred in the Indian Ocean. Such a large movement of sea water will inevitably modify the Earth’s gravity field.

The atmospheric pressure data are from the European Centre for Medium-Range Weather Forecasts (ECMWF). The data are monthly averaged atmospheric pressures on a $2.5^\circ \times 2.5^\circ$ grid and cover the same period as that of T/P SLAs. We first computed a global mean pressure field by averaging all data. Monthly atmospheric pressure anomalies (APAs) were then obtained by subtracting the mean pressure from individual monthly pressures. Fig. 2 shows APAs in December 1997. As seen in Fig. 2, it is typical that in December atmospheric pressure highs occur over major continents of the northern hemisphere and lows occur over major continents of the southern hemisphere.

5.2. Analysis: time series of J_2 variation

The global grids of CSLA and APA over the period from January 1993 to October 2001 were expanded into

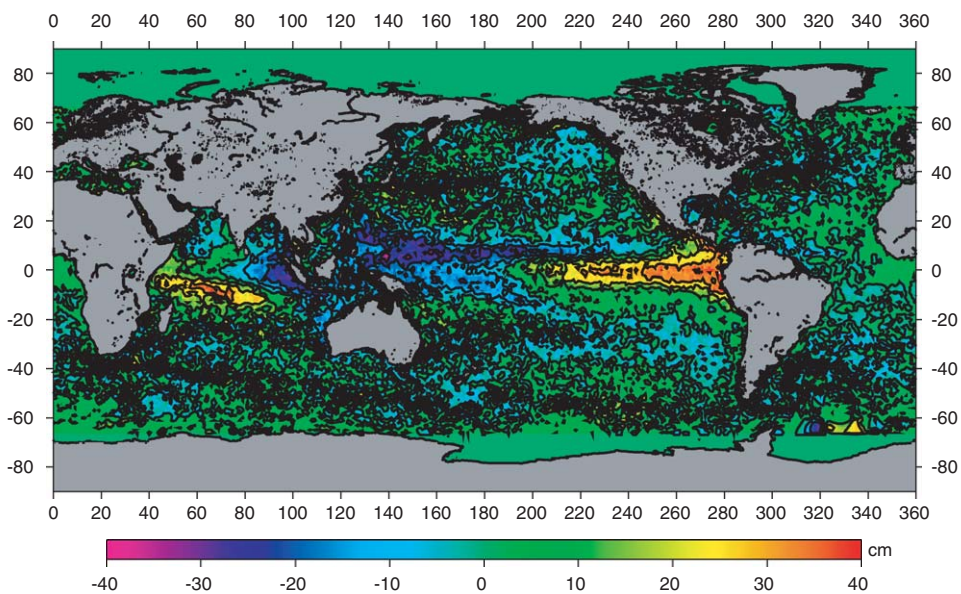


Fig. 1. Monthly averaged corrected sea level anomaly (CSLA) from T/P in December 1997.

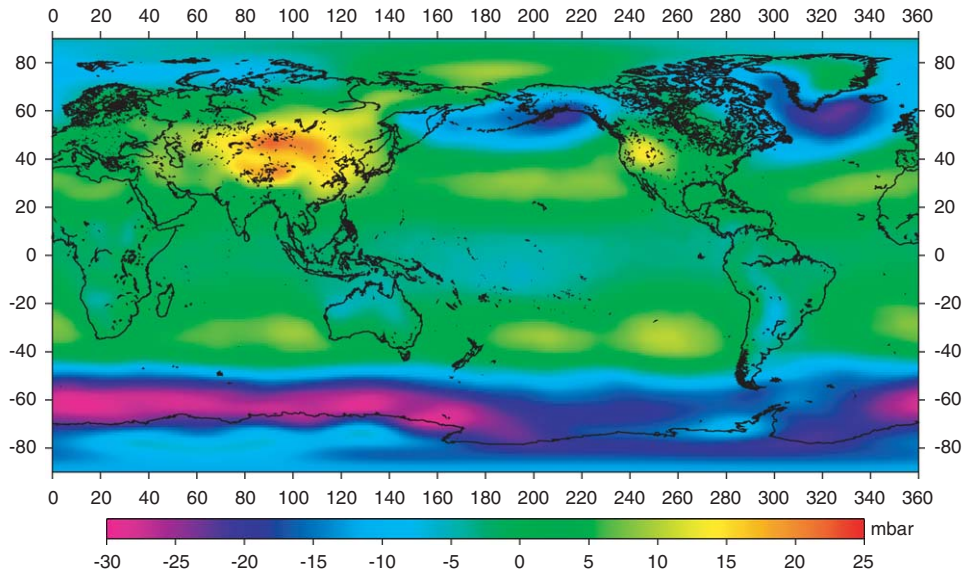


Fig. 2. Monthly averaged atmospheric pressure anomaly in December 1997.

spherical harmonic series up to degree 50 using program sha. The results are changes of geopotential coefficients due to oceanic and atmospheric mass redistributions. The time series of a harmonic coefficient can be used to investigate long-term variations of certain geophysical phenomena. For example, the degree-zero coefficient represents the total mass change of the underlying geophysical fluid (water or atmosphere). The degree-one coefficients are associated with the variation of geocenter. The degree-two coefficients have to do with the variations of the Earth's flattening (the zonal term, $\Delta\bar{J}_{20}$), polar motions (the tesseral terms, $\Delta\bar{J}_{21}, \Delta\bar{K}_{21}$) and principal moments of inertia (the sectorial terms, $\Delta\bar{J}_{22}, \Delta\bar{K}_{22}$); see Heiskanen and Moritz (1985). As an example, Fig. 3 shows the time series of $\Delta\bar{J}_{20}$ from CSLAs and from APAs. The two time series show strong annual variations and weak semi-annual variations. However, the phases of the annual variations from the two sources are different. In general, the annual peak of CLSA occurs in summer, while the annual peak of APA occurs in winter. The phases of the semi-annual variations from the two sources are also different. Interestingly, the slopes of $\Delta\bar{J}_{20}$ from CSLAs before and after December 1997 are $0.207 \times 10^{-11}/\text{year}$ and $0.361 \times 10^{-10}/\text{year}$, respectively. This phenomenon agrees with the result from satellite laser ranging observations (Cox and Chao, 2002). Such a dramatic change of the trend of the Earth's flattening is believed to be caused by a recent surge in subpolar glacial melting and by mass shifts in the Southern, Pacific, and Indian oceans (Dickey et al., 2002). The slopes of $\Delta\bar{J}_{20}$ from APAs before and after December 1997 are

-0.408×10^{-10} and, -0.608×10^{-10} , respectively, so the rate of change is steady for 1993–2002. Further investigations of the links between the J_2 variation and geophysical phenomena are left to interested readers and will not be elaborated here.

5.3. Synthesis: rate of geoid change

The time series of harmonic coefficients obtained in Section 5.2 were used to compute the rates of change for individual coefficients. The rates were then used in (23) to compute the rates of geoid change up to degree 50. Figs. 4 and 5 show the rates of geoid change from CSLA's and from APAs, respectively. The patterns of geoid rate from the two sources are different. The CSLA-implied geoid change contains a high near the "warm pool" northeast of Australia, where sea water piles up before an El Niño occurs. Also, distinct lows occur in the eastern Pacific Ocean and the western Indian Ocean. The atmospheric pressure-implied geoid change contains distinct highs in the northeastern Pacific Ocean and the East Antarctica, and distinct lows in the waters east of Australia and the Southeast Pacific Basin. Again, investigations of the phenomena seen in Figs. 4 and 5 are left to interested readers.

6. Conclusions

This paper presents FFT-based methods for spherical harmonic analysis and synthesis. Two efficient computer programs coded in FORTRAN have been developed

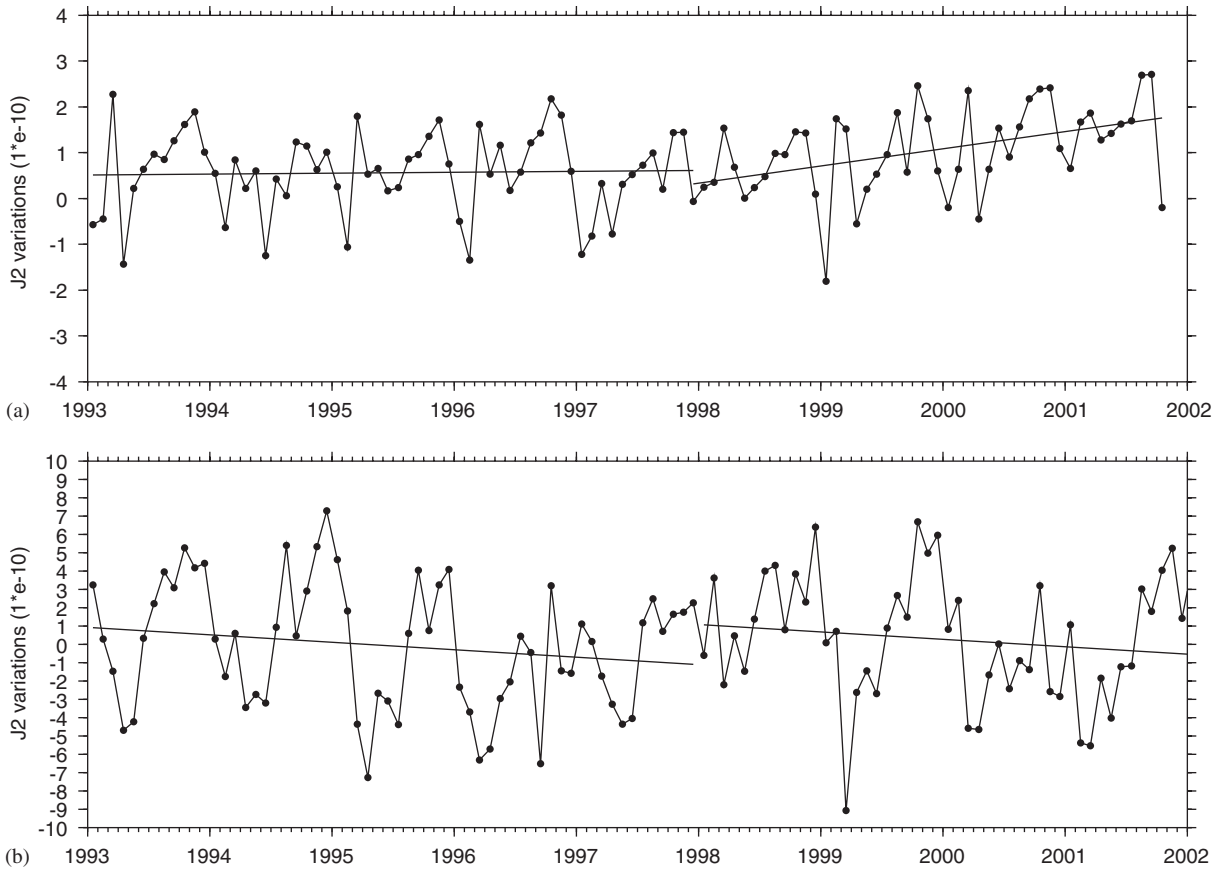


Fig. 3. Time series of J_2 variation due to mass changes in (a) ocean, and (b) in atmosphere.

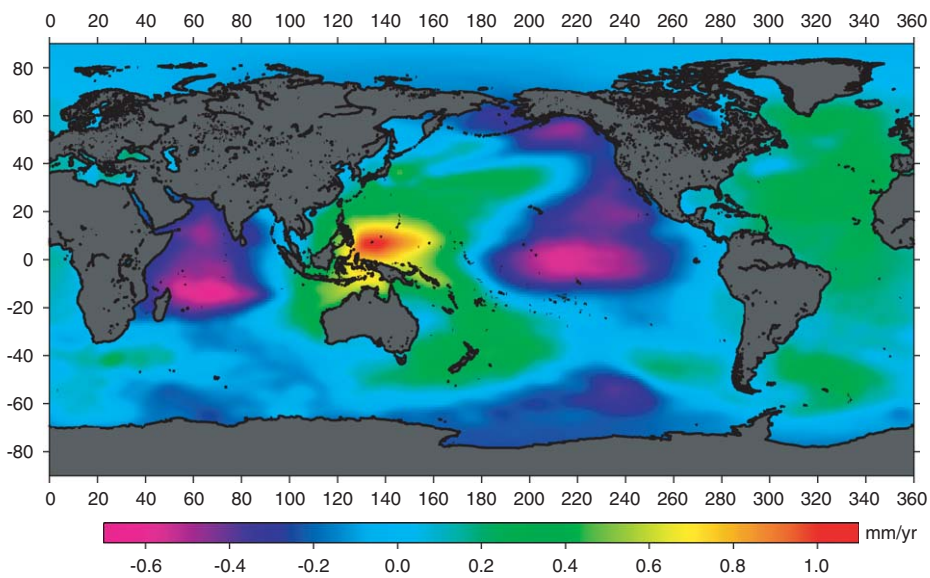


Fig. 4. Rates of geoid change due to oceanic mass change.

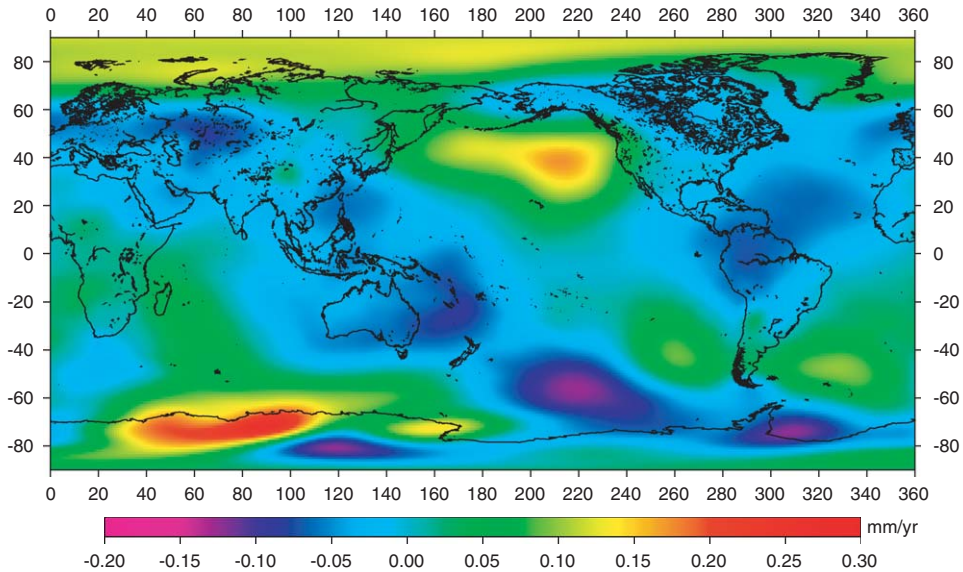


Fig. 5. Rates of geoid change due to atmospheric mass change.

based on the proposed methods. Both general cases and special cases of analysis and synthesis were investigated. The special cases involve the Earth's gravity field. We demonstrate these computer programs using sea level data from T/P and atmospheric data from ECMWF. Interesting phenomena have been found in the J_2 time series and the rates of geoid change. The programs developed in this paper can facilitate the analysis and synthesis of temporal gravity variations from satellite missions such as GRACE.

Acknowledgments

This research is supported by the National Space Organization (NSPO), Taiwan/ROC, under the project "Determination and analysis of Earth's gravity field using COSMIC GPS data". We are grateful to JL Chen of Center for Space Research, Austin, for supplying the steric heights, and to two anonymous reviewers for their constructive comments.

Appendix A. Usages of computer programs sha and syn

The usage of sha is

```
sha file.grd3 -Gcoef_file -TtypeId [-C -Ddensity -Lnmax -Kloadnumbers.txt]
```

where

file.grd3: input file of grd3 grid containing data (must cover the entire sphere)

-G: output file of fully normalized harmonic coefficients

-T: type of gridded data

1 = height change of hydrological origin (e.g. sea level, water table, snow, ice) (unit: m)

2 = pressure anomaly (unit: mbar)

3 = arbitrary surface function (e.g., SST, height) (unit: m)

Options:

-C: harmonic coefficients will not be normalized [default: fully-normalized]

-D: density (in kg/m^3) associated with height change of hydrological origin [default: 1000]

-K: file of loading Love numbers [default: Han and Wahr (1995) up to degree 696]

-L: maximum degree of spherical harmonic expansion [default: $\pi/\Delta\theta$]

The usage of syn is

```
syn coef_file -Idx/dy -Gfile.grd3 -Lnmax -Ttype [-Aa -B -Dr -Mgm -R]
```

where

coef_file: input file of harmonic coefficients

-I: sampling (grid) interval (in degrees) along longitude and latitude

-G: output file of global grid in .grd3

-L: maximum degree of spherical harmonic expansion

-T: type of value to compute

0 = geoidal height

1 = gravity anomaly

2 = arbitrary function

Options:

- A: scaling factor (*a*) associated with harmonic coefficients [default: $a = 6378136.3$ m]
- B: file of harmonic coefficient is a binary file [default: ascii]
- D: radius (in meter) of sphere on which the expansion is made [default: $r = a = 6378136.3$ m]
- M: product of Newtonian constant and the mass of the earth [default: $3986004.415 \times 10^8 \text{ m}^3/\text{s}^2$]
- R: subtract geopotential coefficients of the GRS80 ellipsoid from the input coefficients [default: do not subtract]

Appendix B. Batch job of spherical harmonic analysis using CSLAs

- (1) Interpolate along-track CSLAs onto a global $1^\circ \times 1^\circ$ grid using GMT's "surface" surface tp_1997_12.xyh -R0/360/-90/90 -I1/1 -T0 -Gtemp.grd
- (2) Convert the GMT grd grid to a grd3 grid grd2xyz temp.grd -Z | z2grd3 -R0/360/-90/90 -I1/1 -Gtemp.grd3
- (3) Perform spherical harmonic analysis to degree 50 using sha sha temp.grd3 -L50 -T1 -D1000 -Gtp_1997_12.coe

Appendix C. Batch job of spherical harmonic synthesis using rates of geopotential coefficients

- (1) Compute rates of geoid change on a global $1^\circ \times 1^\circ$ grid using rates of geopotential coefficients up to degree 50
syn tp_coe_rate.dat -L50 -I1/1 -T0 -Gtemp.grd3
- (2) Convert the grd3 grid to a GMT netcdf grid
grd3toz temp.grd3 | xyz2grd -Z -R0/360/-90/90 -I1/1 -Gtp_coe_rate.grd

References

Archivings Validation and Interpretation of Satellite Oceanographic data (AVISO), 1996. AVISO User Handbook for Merged TOPEX/Poseidon Products, Edition 3.0, Centre National d'Etudes Spatiales, Toulouse, 196pp.

Chen, J.L., Wilson, C.R., Hu, X.G., Zhou, Y.H., Tapley, B.D., 2004. Oceanic effects on polar motion determined from an ocean model and satellite altimetry: 1993–2001. *Journal of Geophysical Research* 109, Art. No. B0241.

Colombo, O.L., 1981. Numerical methods for harmonic analysis on the sphere. Report No. 310, Department of Geodetic Science and Surveying, The Ohio State University, Columbus, Ohio, 139pp

Cox, C.M., Chao, B.F., 2002. Detection of a large-scale mass redistribution in the terrestrial system since 1998. *Science* 297, 831–833.

Dickey, J.O., Marcus, S.L., de Viron, O., Fukumori, I., 2002. Recent Earth oblateness variations: unraveling climate and postglacial rebound effects. *Science* 298, 1975–1977.

Dilts, G.A., 1985. Computation of spherical harmonic expansion coefficients via FFT's. *Journal of Computational Physics* 57, 439–453.

Engelis, T., 1985. Spherical harmonic expansion of the Levitus sea surface topography. Report 385, Department of Geodetic Science and Surveying, The Ohio State University, Columbus.

Han, D.Z., Wahr, J., 1995. The viscoelastic relaxation of a realistically stratified Earth, and a further analysis of postglacial rebound. *Geophysical Journal International* 120, 287–311.

Healy Jr., D., Rockmore, D., Kostelec, P., Moore, S., 2003. FFTs for the 2-sphere—improvements and variations. *Journal of Fourier Analysis and Applications* 9, 341–385.

Heiskanen, W.A., Moritz, H., 1985. *Physical Geodesy*. Reprint, Institute of Physical Geodesy, TU Graz, 364pp.

Hwang, C., 2001. Gravity recovery using COSMIC GPS data: application of orbital perturbation theory. *Journal of Geodesy* 75, 117–136.

Kostelec, P., Maslen, D., Rockmore, D., Healy Jr., D., 2000. Computational harmonic analysis for tensor fields on the two-sphere. *Journal of Computational Physics* 162, 514–535.

Lemoine, F.G., Kenyon, S.C., Factor, J.K., Trimmer, R.G., Pavlis, N.K., Chinn, D.S., Cox, C.M., Klosko, S.M., Luthcke, S.B., Torrence, M.H., Wang, Y.M., Williamson, R.G., Pavlis, E.C., Rapp, R.H., Olson, T.R., 1998. The Development of Joint NASA GSFC and the National Imagery and Mapping Agency (NIMA) Geopotential Model EGM96. Report NASA/TP-1998-206861, National Aeronautics and Space Administration, Greenbelt, MD, 575pp.

Mohlenkamp, M.J., 1999. A fast transform for spherical harmonics. *Journal of Fourier Analysis and Applications* 5, 159–184.

Paul, M.K., 1978. Recurrence relations for integrals of associated Legendre functions. *Bulletin Géodésique* 52, 177–190.

Potts, D., Steidl, G., Tasche, M., 1998. Fast and stable algorithms for discrete spherical Fourier transforms. *Linear Algebra and Its Applications* 275–276, 433–450.

Rapp, R.H., 1989. Combination of satellite, altimetric and terrestrial gravity data. In: Sanso, F., Rummel, R. (Eds.), *Theory of Satellite Geodesy and Gravity Field Determination*. Lecture Notes in Earth Sciences, vol. 25. Springer, Berlin, pp. 261–284.

Suda, R., Takami, M., 2002. A fast spherical harmonics transform algorithm. *Mathematics of Computation* 71, 703–715.

Tapley, B.D., Bettadpur, S., Ries, J.C., Thompson, P.F., Watkins, M.M., 2004. GRACE measurements

- of mass variability in the Earth system. *Science* 305, 503–505.
- Torge, W., 1989. *Gravimetry*. de Gruyter, Berlin, 465pp.
- Wahr, J., Molenaar, M., Bryan, F., 1998. Time variability of the Earth's gravity field: hydrological and oceanic effects and their possible detection using GRACE. *Journal of Geophysical Research* 103, 30205–30229.
- Wessel, P., Smith, W.H.F., 1995. New version of the Generic Mapping Tool released. *Eos Transaction, (American Geophysical Union)* 76, 329.